Application of a seismic network to baleen whale call detection and localization in the Panama basin – a Bryde's whale example

Jean Baptiste Tary[1,2,a], Christine Peirce[3], Richard W. Hobbs[3], Felipe Bonilla Walker[1], Camilo De La Hoz[1,4], Anna Bird[3], Carlos Alberto Vargas[5]

[1] *Departamento de Geociencias, Universidad de los Andes, Bogotá, Colombia*

[2] *Now at Geophysics section, School of Cosmic Physics, Dublin Institute for Advanced Studies, Dublin, Ireland*

[3] *Department of Earth Sciences, Durham University, Lower Mountjoy, South Road, Durham, DH13LE, UK*

[4] *Now at Department of Physics, University of Alberta, Edmonton, Canada*

[5] *Departamento de Geociencias, Universidad Nacional de Colombia, Bogotá, Colombia*

Abstract

Baleen whales use sounds of various characteristics for different tasks and interactions. This study focuses on recordings from the Costa Rica Rift, in the Eastern Tropical Pacific Ocean, made by 25 ocean-bottom seismographs and a vertical array of 12 hydrophones between January and February 2015. The whale calls observed are of two kinds: more commonly, repetitive 4-5 s long signals separated into two frequency bands centered at ~20 and ~36 Hz; less commonly, a series of ~0.5-1.0 s long, lower amplitude signals with frequencies between 80 and 160 Hz. These characteristics are similar to calls attributed to Bryde's whales which are occasionally sighted in this region. In this study, the repetitive calls are detected using both the STA/LTA approach and a network empirical subspace detector. In total, 188 and 1891 calls are obtained for each method, demonstrating the value of the subspace detector for highly similar signals. These signals are first localized using a non-linear grid search algorithm and then further relocalized using the double-difference technique. The

[a] Email: tary@cp.dias.ie

high-resolution localizations reveal the presence of at least seven whales during the recording period, often crossing the instrument network from southwest to northeast.

I. INTRODUCTION

In water, the exchange of information by sight and smell is only possible over small distances. Instead, many marine animals, and marine mammals in particular, have developed ways of exchanging information using vibration and sound. Approaches include vocalizations, such as calls and songs, and non-vocal sounds, for example generated by tail and fin slapping (*Kavanagh et al., 2017*). Marine mammals use these sounds for various purposes such as communicating, foraging and socializing (e.g., *Frankel, 2009*; *McDonald et al., 2006*). Cetacean vocalizations, in particular, have a wide range of signal characteristics, including waveform shape and frequency content (e.g., *Richardson et al., 2013*; *Frankel, 2009*). The frequency characteristics of baleen whale vocalizations vary from several Hz for Blue whales (*Balaenoptera musculus*) to more than 20 kHz for Humpback whales (*Megaptera novaeangliae*), and call durations can range from a few tenths of a second to few tens of seconds (*Frankel, 2009*).

In the Eastern Tropical Pacific Ocean, where the Costa Rica Rift (CRR) is located (Figure 1), various baleen whale species have been encountered, including Humpback whales, Bryde's whales (*Balaenoptera brydei* and *Balaenoptera edeni*), Minke whales (*Balaenoptera acutorostrata*), Fin whales (*Balaenoptera physalus*), Sei whales (*Balaenoptera borealis*), and Blue whales (*Wade & Gerrodette, 1993*; *Palacios et al., 2012*). These species have different abundances and vulnerability levels in this region, but experience the same threats corresponding to climate change, animal bycatch, ghost nets, ship noise and ship strike (*Palacios et al., 2023*). Baleen whales are vocal in the frequency range of seismometers, geophones and hydrophones which could, thus, provide a way of monitoring their distribution and behavior. Such low frequency (<100 Hz) sound emissions can propagate over several hundred kilometers, due to the relatively low sound attenuation in water and the presence of a low-velocity waveguide in the water column. However, increase in ship noise may mask such communications, and might induce changes in their vocalizations (*McDonald et al., 2009*; *Hatch et al., 2012*).

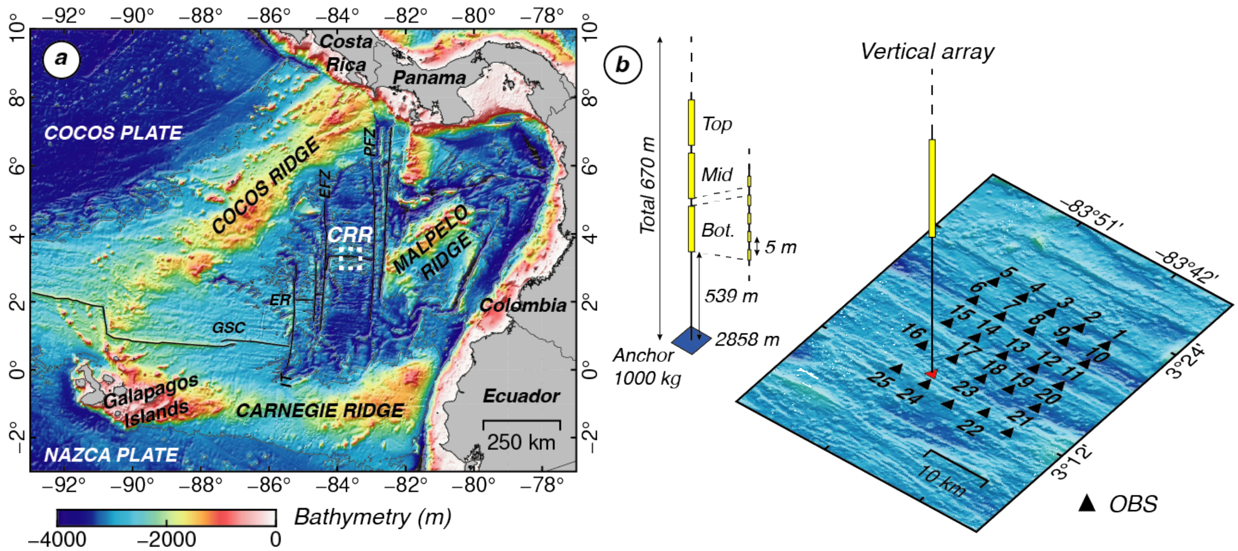

FIG. 1. (Color online). a) Bathymetric map of the Panama Basin, showing the position of the Costa Rica Rift (CRR). GSC: Galapagos Spreading Center, IT: Inca Transform, ER: Ecuador Ridge, EFZ: Ecuador Fracture Zone, PFZ: Panama Fracture Zone. b) Zoom-in of the grid of OBSs (numbered black triangles) and on the VA (red triangle) deployed close to the CRR (white dashed box in (a)). The construction of the VA is shown between maps. Hydrophone positions are indicated by yellow shaded sections.

Passive acoustic monitoring of whales using acoustic instruments informs knowledge of their ecology and the possible impact of anthropogenic noise. Such approaches can also monitor, over the long term, large portions of the oceans, but they are costly and large gaps in coverage remain (*Wilcock & Hilmo, 2021*). Ocean-bottom seismograph (OBS) deployed for other purposes (e.g., seismic surveys, seismicity monitoring), can also provide complementary monitoring data (e.g., *McDonald et al., 1995*; *Dunn & Hernandez, 2009*; *Brodie & Dunn, 2015*). To contribute to the study of whales in the Eastern Tropical Pacific Ocean region, we take advantage of the deployment of ocean-bottom seismographs and hydrophones close to the CRR in the Panama basin (*Hobbs & Peirce, 2015*) (Figure 1). These instruments were originally deployed to study the lithospheric structure of the CRR and its surroundings using mainly seismic data (e.g., *Wilson et al., 2019*; *Robinson et al., 2020; Funnell et al., 2021; Peirce et al., 2023*). More specifically, we here focus on the analysis of whale calls observed in the data of the North Grid (NG) where 25 closely-spaced OBSs and a vertical array (VA) of 12 hydrophones were deployed in January-February 2015 (Figure 1).

Whale calls are generally detected using energy-based methods, spectrogram correlation (*Širović et al., 2004*) and template matching (*Socheleau et al., 2015; Matias & Harris, 2015*). Here, we use the STA/LTA (short-term average/long-term average) approach and, taking advantage of the high whale call similarity, a network empirical subspace detector (*De La Hoz et al., 2021*) to detect the whale calls. The STA/LTA algorithm is based on the ratio of the average of signal values calculated for a short sliding window and a long sliding window. The subspace detector uses a basis of signal vectors to detect other similar signals, by calculating the decomposition of a range of similar signals projected onto the continuous data (*Harris, 2006*). We then localize the identified whale calls using a non-linear grid search algorithm and the timing differences observed between different geophones and hydrophones (*Lomax et al., 2009*). In our study the calls are highly similar and recorded by a dense network of OBSs, thus, we can also refine the localizations, to high resolution, using the double-difference method (*Waldhauser & Ellsworth, 2000*). We then analyze the call characteristics and their spatio-temporal distribution, providing detailed information on signals and whale behaviors, which is fundamental for their identification, management and conservation.

II. DATA AND METHODS

A. Data acquisition

This study uses data recorded by OBSs and a vertical array of hydrophones provided by the UK's OBIF (Ocean-Bottom Instrumentation Facility – see Acknowledgements) and deployed during RRS James Cook cruise JC114 of the OSCAR research project (*Hobbs & Peirce, 2015*). The primary objectives of this deployment were to image the oceanic crust around the CRR and study fluid interactions between crust and the ocean through the acquisition of multi-channel seismic reflection data and wide-angle seismic profiles (e.g., *Gregory, 2018*; *Wilson et al., 2019*; *Robinson et al., 2020*; *Funnell et al., 2021*; *Peirce et al., 2023*). The acquired data, thus, has periods with and without active-source seismic operations. During the non-active shooting periods, the passive recordings provide valuable information for seismic attenuation estimates (*Vargas et al., 2018*) and the degree of the natural microseismicity (*Lowell et al., 2020*; *Tary et al., 2021*). In this study, we focus on the detection and localization of the whale calls that were also recorded.

The OBSs were deployed ∼5 km apart on the seafloor within an ~20 x ~20 km footprint, and the VA was deployed in the southwest corner of this grid (Figure 1). The overall recording period ran between 26th January and 17th February 2015, although individual instruments have different recording periods due to their respective recovery times. All but five OBSs (OBSs 4, 7, 14, 17, 24) were recovered on 1st and 2nd February. The remaining five OBSs as well as the VA were recovered later on 16th and 17th February. The deepest hydrophone of the VA was positioned at 539 m above the seafloor (at approximately 2858 m depth below sea surface), with the remainder spaced at ~5 m intervals upwards through the water column (i.e., over 55 m). One of these hydrophones did not record any useful data, most likely due to it being detached from the datalogger by strong lateral surface currents during deployment (*Hobbs & Peirce, 2015*). Each OBS and the VA had High Tech HTI-90-U hydrophones, with the OBSs also having, in addition, a three-component (3-C), short-period geophone set comprising Sercel L-28 4.5 Hz sensors. The data streams were sampled at 500 Hz. All instrument clocks were synchronized to GPS before deployment and on recovery, and any drift was linearly corrected.

Although the airgun active-source seismic shots (GI, G, and Bolt array) hinder the detection of natural occurring signals such as the microseismicity, whale calls have different signatures (i.e., waveform and frequency content), and are generally observed by multiple stations given the dense instrument distribution (Figure 2), improving the ability to reliably detect and localize these signals.

B. Whale call detections

We initially analyzed the dataset to detect the microseismicity (*Tary et al., 2021*), using the STA/LTA algorithm applied to band-pass filtered (between 5 and 120 Hz) geophone OBS data (vertical component). Together with 1061 microearthquakes, we also detected whale vocalizations with very similar signal characteristics (e.g., Figure 2). Considering the main signal frequency components of these vocalizations, at ~20 and ~36 Hz, we re-applied the STA/LTA algorithm to the same data, but instead filtered it between 20 and 45 Hz to remove as much background noise as possible. To identify whale calls we used short and long windows of 3.0 and 15.5 s, respectively, and recorded potential events when the STA/LTA ratio exceeded 3 at a minimum of three stations within a time window of 10 s. The potential events were then manually reviewed to select the events corresponding to whale calls.

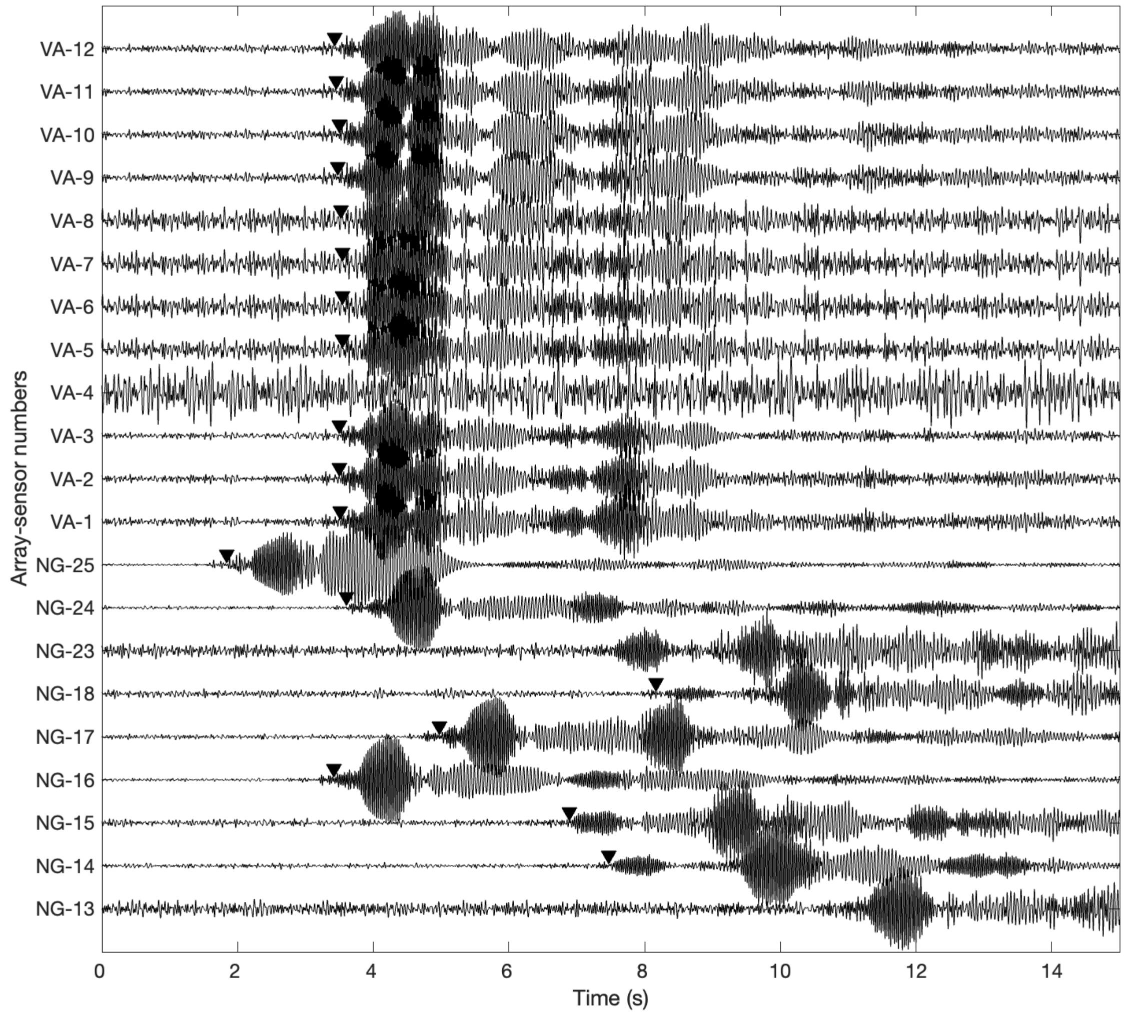

FIG. 2. Typical whale call recorded by the hydrophones of the vertical array (VA) and a selection of OBS hydrophones (NG-), band-pass filtered between 10 and 45 Hz. P-wave time picks are indicated by the black inverted triangles. The call origin time is 29th January 2015, at 15:30:24.

Taking advantage of the high signal similarity, we then applied the empirical subspace detector to these detections (*Barrett & Beroza, 2014*). Contrary to the match filter where each previously detected signal is used as a template to detect new events, the subspace detector employs the previously detected signals to produce new signal subspace bases defined by a set of orthonormal signal vectors $\mathbf{U}$ (*Harris, 2006*). The original signals are first separated into different clusters, which are then used to calculate the subspace bases. The waveforms in each cluster in matrix $\mathbf{A}$ are aligned on the P-wave arrival based on their cross-correlation coefficient, and the subspace base and its orthonormal signal vectors are given by the singular value decomposition of matrix $\mathbf{A}$ as

$$\mathrm{SVD}(\mathbf{A}) = \mathbf{USV}^{\mathrm{T}}, \tag{5}$$

where $\mathbf{U}$ is also the matrix of left-singular vectors, and $\mathbf{S}$ and $\mathbf{V}$ are the singular values and right-singular vectors, respectively. Then, only a small selection of left-singular vectors $\mathbf{U_s}$, based on the fraction of the total signal energy they represent for example (*Harris, 2006*; *Song et al., 2014*), is used for detection. The different segments s of continuous data are then projected onto the matrix $\mathbf{U_s}$ to define the detection metric of the subspace detector z following

$$z = \frac{s^{\mathrm{T}}\mathbf{U_s}\mathbf{U_s^{\mathrm{T}}}s}{s^{\mathrm{T}}s}. \tag{6}$$

Contrary to the subspace detector, the empirical subspace detector uses the stack of matrix $\mathbf{A}$ and the first derivative of the stack with respect to time to populate $\mathbf{U_s}$ instead of a selection of left-singular vectors. The stack and its first derivative closely resemble the first two left-singular vectors, and using those instead of left-singular vectors can lead to a higher number of detections (*Barrett & Beroza, 2014*). The detection is performed using the continuous hydrophone data, both from the OBSs and the VA, band-pass filtered between 10 and 45 Hz. To take advantage of the dense array of hydrophones, we use a network detection metric corresponding to the sum of the detection metrics z over all stations in the network (*De La Hoz et al., 2021*). We sum the maximum of the detection metrics z within a sliding window of 5 s to account of event moveout. The detection threshold γ_c was defined using correlations between the events in matrix $\mathbf{A}$ and random segments of continuous data containing only noise (*Song et al., 2014*). This threshold was then adjusted by reviewing detection results using representative data. We manually selected the detected events corresponding to whale calls. The whale calls were picked automatically using the maximum of the cross-correlation with the stack of matrix **A**, with the picks saved only if their cross-correlation coefficients were greater than 0.65. These time picks were subsequently confirmed manually.

C. Localization methods

1. Absolute localizations

Absolute event localizations were obtained using NonLinLoc (*Lomax et al., 2001*, *2009*), which uses non-linear methods to search for the global maximum of the localization probability density function. In most cases, the whale calls observed correspond to a P-wave travelling from the source to the instruments through the water. Theoretical P-wave travel-times were computed using the eikonal equation, which provides travel-times for the first, high-frequency wave to connect potential sources and receivers. The crust was not included in the velocity model used for this calculation as this leads the algorithm to calculate the faster crustal arrivals instead of water-borne arrivals. The water column velocity model used was derived from a 1D average of conductivity-temperature-depth (CTD) measurements in the vicinity of the CRR (*Banyte et al., 2018a,b*) (Figure 3). This 1D velocity model extends to a water depth of ~3.12 km, and was then linearly extrapolated to a maximum depth of 3.5 km. The final 3D localization model consists in a grid of 60 x 60 x 3.5 km with node spacings of 0.1 km in all dimensions.

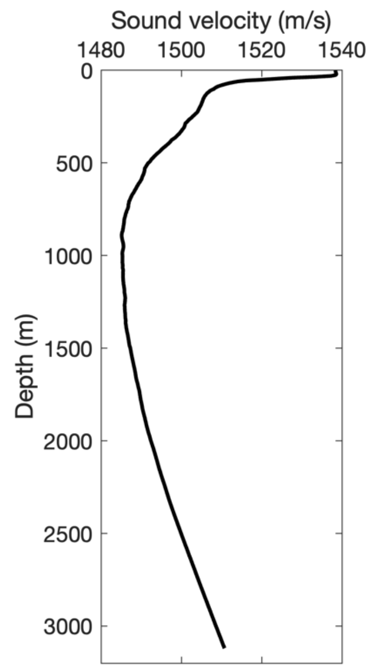

FIG. 3. Sound velocity profile in the water column calculated by averaging CTD measurements obtained in the vicinity of the CRR (*Banyte et al., 2018a, 2018b*). This 1D profile was used to construct the 3D localization velocity model.

The calculated direct arrival travel-times may not correspond to the arrivals recorded by each instrument due to strong bathymetric changes obstructing the direct wavepath, leading to multi-pathing (*Dréo et al., 2019*). This is especially the case for large source-receiver distances. In our case, however, most of the OBSs recording the whale calls are located less than 10-15 km from the whale's position. In addition, travel-time picks associated with large travel-time residuals are down-weighted during the localization procedure. This increases the robustness of the localization procedure, focusing on high-quality travel-time picks closer to the source location. Time pick uncertainties are also automatically attributed to each travel-time pick depending on the signal-to-noise ratio. After selecting events with a minimum of four phase picks, the localization is finally determined using the equal-differential time likelihood function and the oct-tree importance sampling method (*Lomax et al., 2009*). In the present case, including travel-time residuals as station corrections to mitigate the effects of potentially unaccounted for velocity changes and ray paths, did not improve the localizations. Spatial uncertainties were estimated using the dimensions of the 68% confidence ellipsoid fitting the probability density function of each event localization (*Lomax et al., 2009*).

2. Double-difference relative localizations

Using the travel-time picks and the absolute localizations obtained with NonLinLoc, we then relocalize the events using the double-difference method implemented in hypoDD (*Waldhauser & Ellsworth, 2000*), which assumes that similar events recorded by the same seismic station share similar source mechanisms and wave propagation paths from their sources to the receiver(s). Such methods have been successfully applied to the relocalization of Fin whale calls (*Wilcock, 2012*) and acoustic sources (*Tenorio-Hallé et al., 2017*). The double-difference method particularly, which was developed for clusters of similar events, assumes that small observed travel-time pick differences between events at a station are due to small differences in their localizations, and not due to unmapped velocity changes along their propagation paths or in their hypocentral area. This method also benefits from the calculation of high-precision differential travel-time picks based on cross-correlating the event waveforms. In the present case, all observed calls were highly similar indicating a similar source and little impact of the wave propagation on the frequency content of the observed signals. As the travel-time picks had already been obtained using cross-correlation between a high signal-to-noise ratio version of the signal (i.e., the event stack) and event waveforms, we used those picks to calculate the differential timings and did not repeat the event waveform cross-correlation.

With the double-difference method, instead of localizing the events based on their travel-times, events were relocalized relative to each other by calculating the difference in relative timings at the stations (*Waldhauser & Ellsworth, 2000*), as

$$dr_k^{ij} = \left(T_k^i - T_k^j\right)^{obs} - \left(T_k^i - T_k^j\right)^{calc},$$

where i and j are the indexes of two events, recorded at station k, and obs and $calc$ refer to travel-times T observed and calculated, respectively. For events that are closely located with respect to variations in the velocity structure, these differences in relative timings can be related to changes in event locations as

$$dr_k^{ij} = \frac{\partial T_k^i}{\partial \mathbf{m}} \Delta \mathbf{m}^i - \frac{\partial T_k^j}{\partial \mathbf{m}} \Delta \mathbf{m}^j,$$

where $\mathbf{m}$ include the model parameters (x, y, z, and T_0 the origin time), ${\partial T}/_{\partial \mathbf{m}}$ corresponds to slowness in the event region, and $\Delta\mathbf{m}$ corresponds to changes in event parameters. Finding the final set of model parameters $\mathbf{m}$, which correspond to the final event locations, is an ill-posed problem due to the presence of errors (i.e., timings and initial locations), poorly linked events and outliers. This problem was, thus, stabilized using regularization, and solved using weighted, damped least-squares as

$$\left\| \mathbf{W} \begin{bmatrix} \mathbf{G} \\ \lambda \mathbf{I} \end{bmatrix} \mathbf{m} - \mathbf{W} \begin{bmatrix} \mathbf{d} \\ 0 \end{bmatrix} \right\|_2 = 0,$$

where *a priori* weights are included in $\mathbf{W}$, $\mathbf{G}$ contains the slowness, the data vector $\mathbf{d}$ contains the double differences, and λ is the regularization parameter.

The *a priori* weights represent the picking quality, corresponding to either the cross-correlation coefficients obtained during automatic picking or 1 for manual picks. The calls were first clustered using a maximum inter-event distance of 10 km and a minimum of six links with other calls. The inverse problem was then solved iteratively using the conjugate gradients method. We used two sets of 15 iterations, sufficient to converge to the final model parameters; the first set having no data re-weighting and the second using data re-weighting to reject and down-weight data associated with large residuals (dynamic cutoff value of 6).

To work with hypoDD, the source configuration has to be adapted as all the sensors were located deeper than the anticipated positions of the sources (whales) and the VA hydrophones were located above the OBS hydrophones. Our solution was to flip the source–receiver configuration upside down, setting the deepest station at 0 m and the others as if they were located in boreholes. In this configuration, hypoDD uses a constant velocity to relocalize the events, and so we use the average of the 1D water column velocity (1.5 km/s) shown in Figure 3.

III. RESULTS

A. Data and signal characteristics

We first calculated average Welch power spectral densities (PSD) to measure the average noise levels over the entire recording period of the VA and its two nearest OBSs (Figure 4). Each hydrophone's data were first converted to units of Pascal. For frequencies between approximately 1 and 30 Hz, noise levels are comparable between the OBSs and VA hydrophones, although variations are observed between the hydrophones (~ ±5 dB), with the OBS hydrophones generally being the noisiest. OBS and VA hydrophones close to the seafloor also exhibit several spectral peaks between 1 and 5 Hz, the one at 1.8 Hz having the highest amplitude. Between 10 and 18 Hz, the VA hydrophone closest to the seafloor (VA-1) has a higher noise level than all the other hydrophones (+5 dB). For frequencies higher than 30 Hz, noise levels for VA-1 and the OBS hydrophones are higher. VA-1 has a noise level similar to that of the OBS hydrophones at up to 60 Hz, approximately 10 dB higher than the other hydrophones, and then exhibits a lower average noise level of just a few dB higher than the other hydrophones. This seems to indicate that environmental conditions close to the seafloor contribute more to the instrument background noise, and that hydrophones located higher up in the water column do not experience higher noise levels induced by deep ocean currents for example. Over the deployment period, average noise levels are higher at the beginning and end (Figure 5). This is likely due to the presence of the research vessel either deploying instruments (25th and 26th January), carrying out the seismic survey (26th January to 1st February, 12th, 13th and 15th February) or recovering the instruments (1st and 2nd February, 16th and 17th February).

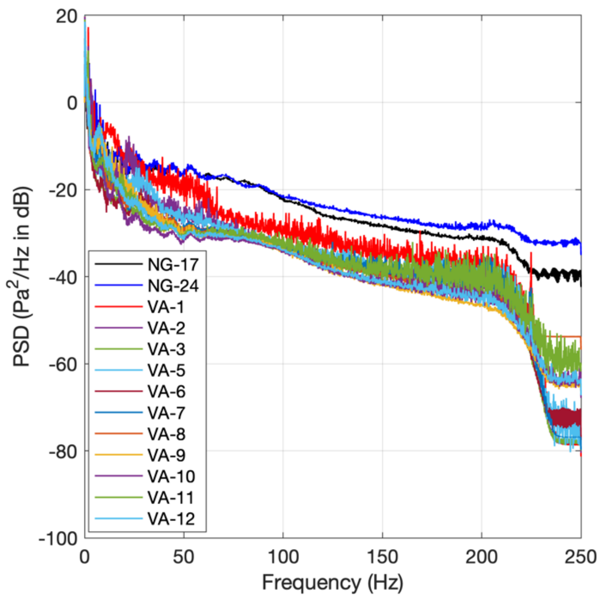

FIG. 4. (Color online). Welch averaged power spectral densities (PSDs) for the whole recording period, for the hydrophones of the two OBSs (NG-17 and NG-24 – Figure 1) closest to the vertical array (VA) and the twelve channels of the VA (in dB re 1 Pa^2/Hz). The data used to calculate the PSDs are in Pascal and unfiltered. We used segment lengths of 300 s with a Hamming window and 50% overlap.

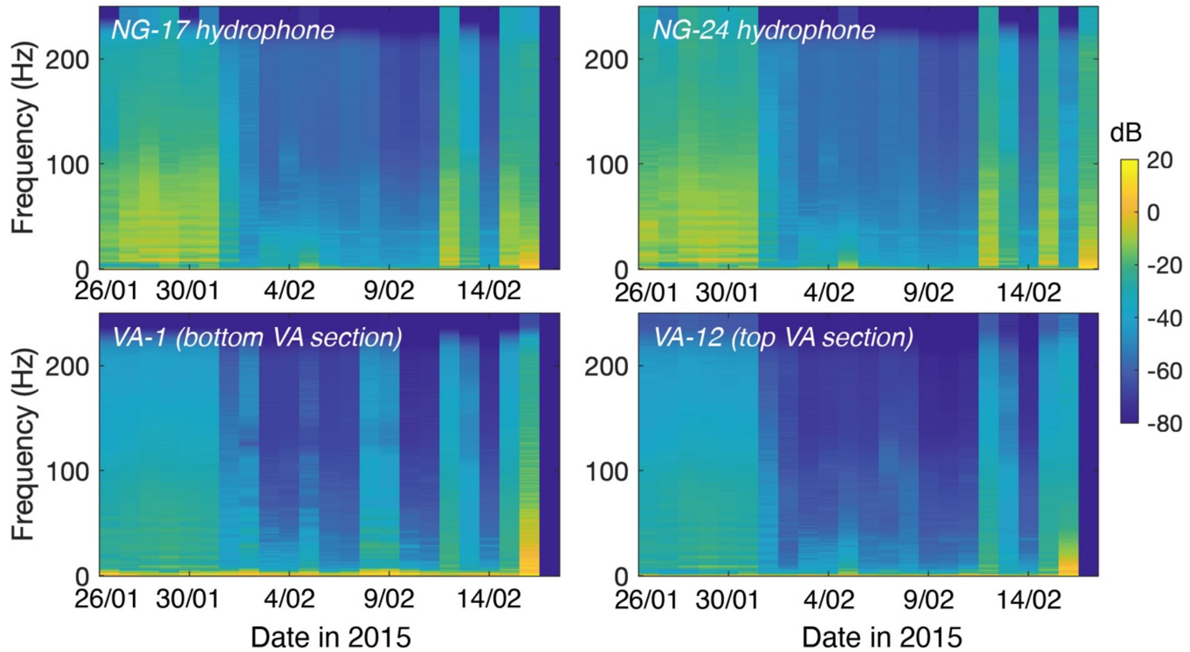

FIG. 5. (Color online). Welch averaged PSDs vs date in 2015 (in dB re 1 Pa^2/Hz) for the hydrophones of OBS NG-17 and NG-24, and VA-1 and VA-12. Over the deployment period, average noise levels are higher at the beginning and end and are thought to be related to the seismic survey (26th January to 1st February, 12th, 13th and 15th February), and deployment (25th and 26th January) and recovery (1st and 2nd February, 16th and 17th February) operations of instruments within the grid.

Whale calls recorded by the VA and OBS hydrophones, although located less than a few kilometers away, display significantly different signals after ~1 s of the first arrival (Figure 2). These differences are most likely due to significantly different wave propagation paths and interferences even for these closely located instruments. For example, the call reflection from the seabed will be part of the received wavelet for the OBSs on the seafloor but will interfere with the direct arrival through the water column at different lag times for the VA hydrophones. Figure 6 shows the time-frequency representation of whale calls with high signal-to-noise ratio using the short-time Fourier transform (e.g., *Tary et al., 2014*). The total signal length is ~4-5 s, and comprises two main parts. The first part starts with a low-amplitude "snout" of ~0.5-1 s, which is only visible for high signal-to-noise ratio signals, followed by a higher-amplitude monochromatic wave packet of ~1 s duration. The frequency of this first part is ~35.7 Hz, together with its overtone at ~71.5 Hz, and the snout potentially also has a frequency closer to 40 Hz (Figure 6). The second part of the signal has large variation in amplitude (i.e., below noise level through to higher amplitude than the first part). Its duration and frequency are roughly 2-3 s and ~20 Hz, respectively. For some of the high-amplitude signals, a high-frequency content up to approximately 150 Hz is also observed in addition to the other two main frequency components (Figure 7). Its magnitude is, however, much lower than those of the main signal components. For these main components, we also observe low-amplitude trails after the main signal (e.g., Figure 7), lasting up to 50 s, likely corresponding to wave multi-pathing within the water column and seafloor.

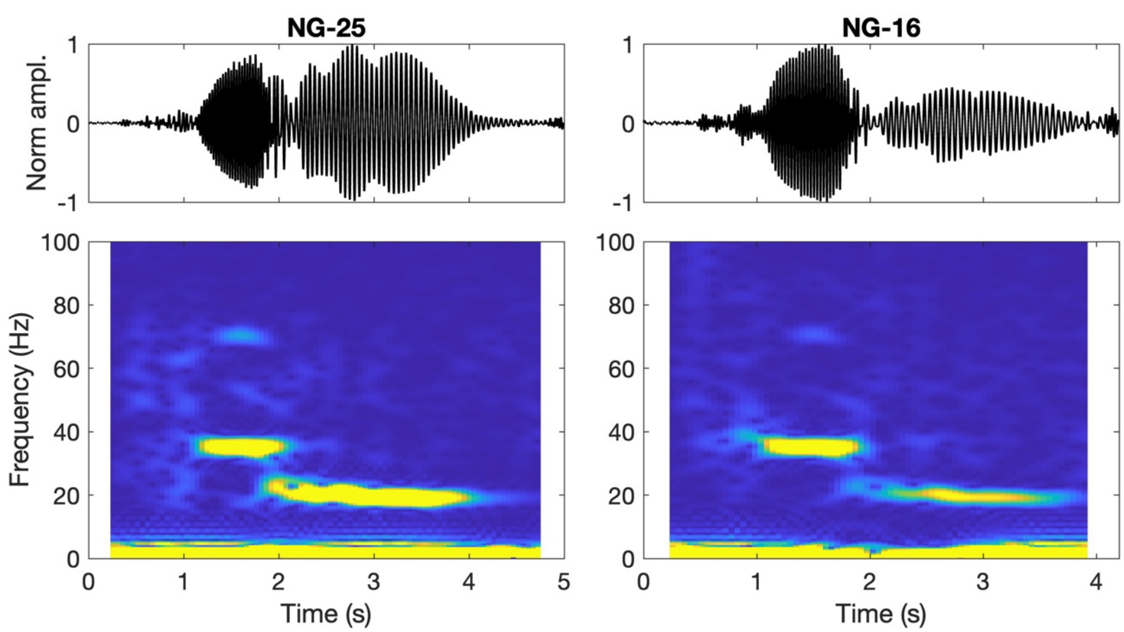

FIG. 6. (Color online). The same whale call, band-pass filtered between 10 and 45 Hz, recorded by the hydrophones of OBS NG-25 (left) and NG-16 (right, see Figure 2) and their time-frequency

representations calculated using the short-time Fourier transform (Hann window of 0.5 s with 90% overlap).

The whale calls are observed in sequences with variable periodicities ranging from tens of seconds to 5-10 min (e.g., Figures 7 and 8), repeated multiple times during the whole survey. At a single instrument, different whale calls can display differences in amplitude reflecting differences in signal strength emitted by the source. However, larger differences are observed between close and distant whale calls, with higher-amplitude calls corresponding to those located close to the instrument and lower-amplitude calls corresponding to answers originating further away. This was verified as several vocal whales were located at different positions within the instrument network during the same time frame (Figure 8). While most of the signals recorded during the survey are similar to those shown in Figures 2 and 6, other signals of higher frequency are also observed (Figure 7 and 9). These are generally clumped in time and with frequency ranging from 80 to 160 Hz. Individually, they are of low amplitude, have a signal-to-noise ratio lower than 3, and a duration of ~0.5-1 s. Despite their lower amplitude, they are still simultaneously recorded by nearby OBSs and some of the VA hydrophones.

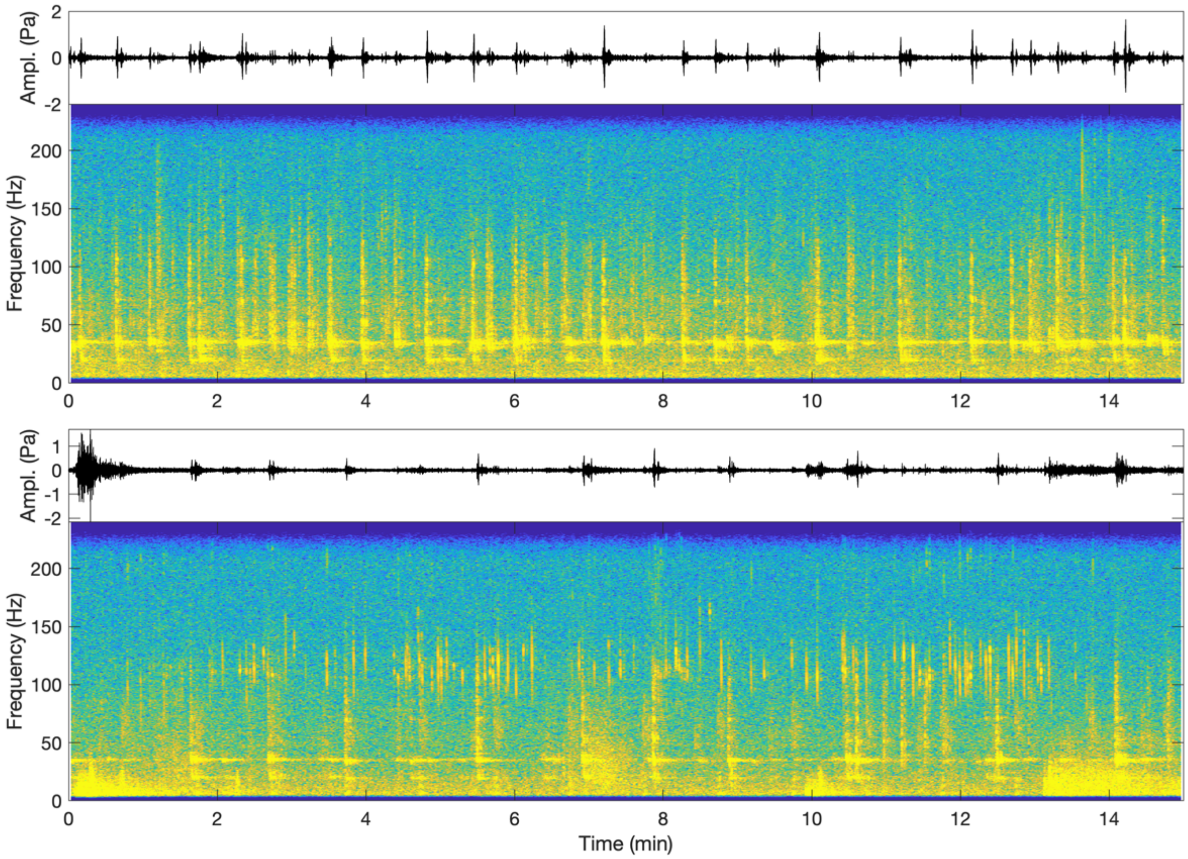

FIG. 7. (Color online). Continuous data from the hydrophone of OBS NG-24 (Figure 1) starting at 00:43:20 (top) and 02:30:00 (bottom) on the 14th February 2015. The time series data are band-pass filtered between 5 and 240 Hz, and the time-frequency representations are calculated using the short-time Fourier transform (Hann window of ~4.1 s with 90% overlap).

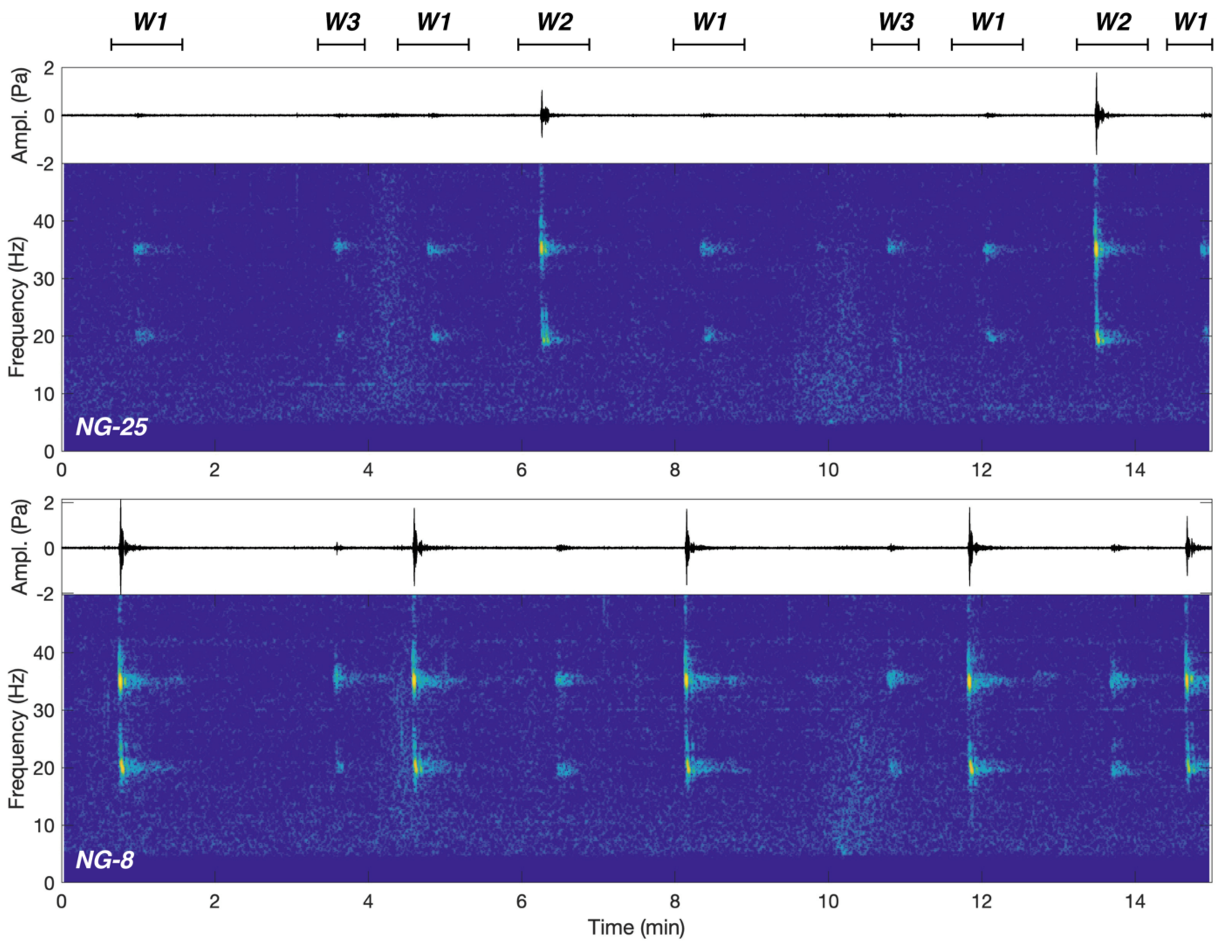

FIG. 8. (Color online). Continuous data from the hydrophones of OBS NG-25 (top) and NG-8 (bottom) (Figure 1) starting at 14:50:50 on the 29th January 2015, band-pass filtered between 5 and 100 Hz. Their time-frequency representations are calculated using the short-time Fourier transform (Hann window of ~4.1 s with 90% overlap). At least three whales are acoustically active (W1, W2 and W3).

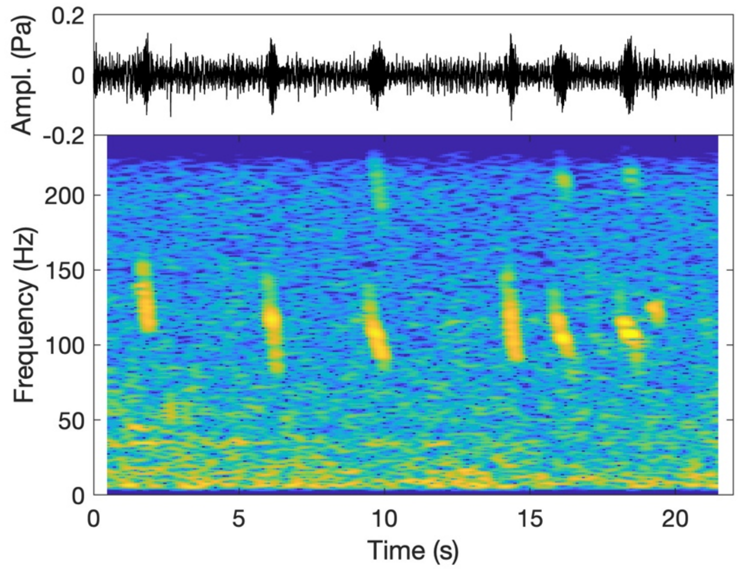

FIG. 9. (Color online). High-frequency whale calls, band-pass filtered between 5 and 240 Hz (top plot), recorded by the hydrophone of OBS NG-24 (zoom-in of Figure 7 between 11 min 50 s and 12 min 13 s) and their time-frequency representation calculated using the short-time Fourier transform (bottom plot, Hann window of ~1 s with 90% overlap).

B. Detection and localization results

Carrying out the detection using the STA/LTA on the vertical geophone component OBS data, we obtained 1177 detections and, from those, manually selected 188 events corresponding to whale calls. The other detections mainly correspond to other coherent signals such as seismic shots and seismicity. By far the majority of these calls were observed on the 29th January, the others being observed during seven other days throughout the whole survey (Figure 10). We then picked the same arrivals using the hydrophone data for both OBSs and VA, resulting in a total of 2134 P-wave picks from the different instruments that recorded the calls. We encountered additional difficulties in manually picking these calls as they share very similar waveform characteristics, whatever their position and distance from the instrument (i.e., similar source and propagation material). Often, more than one arrival moveout at a time is observed, and the emergent low-amplitude snout could be below the noise level. Out of the 188 events, 183 events were localized with average horizontal error, vertical error and RMS travel-time residual of ±2.1 km, ±0.7 km and 0.2 s, respectively (Figure 11). Focusing on the localizations from the 29th January, at least three animals or groups of animals are present simultaneously (see also Figure 8); one stays in the northeast corner of the network, while another passes through the southern half of the network from west to east, and the last moves through the southeast corner of the network to join up with the second at the eastern edge of the network.

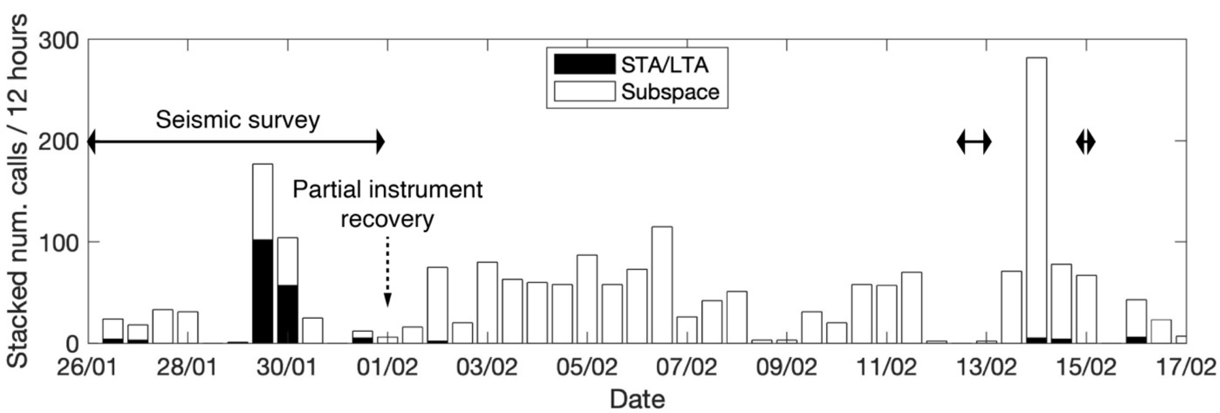

FIG. 10. Temporal distribution of the number of whale calls detected using the STA/LTA (black bars) and the network empirical subspace detector (white bars).

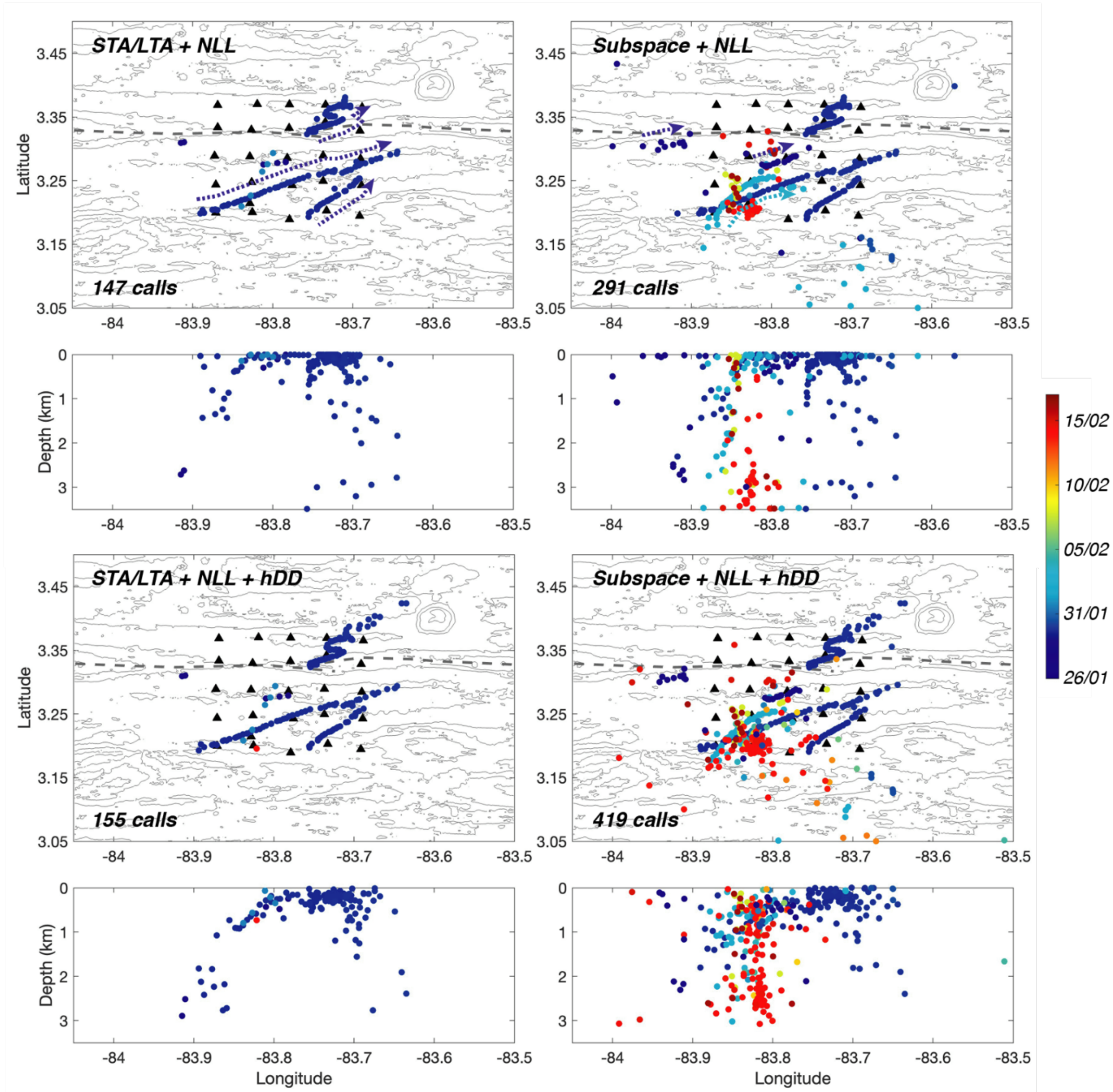

FIG. 11. (Color online). Whale call localizations, laterally and with depth, for the events detected using the STA/LTA and the empirical subspace detector, and localized using NonLinLoc (NLL) and hypoDD (hDD). Only events with horizontal uncertainties lower than $\pm$5 km are shown. The resulting number of events is annotated for each method combination. The dot colors indicate the date after 26th January 2015. Dashed line and black triangles show the location of the CRR and the instruments (OBSs and VA), respectively. Arrows indicate whale trajectories inferred from call timings.

For the empirical subspace detector, we used signals with high signal-to-noise ratio recorded by OBS NG-9 to calculate the stack and its first derivative. Applying the detector to the continuous data we obtain 3100 events for the entire period. We then manually reviewed these detections and selected the 1891 events corresponding to whale calls, including 113 events also detected by the STA/LTA approach. This represents approximately 10 times more events selected using the empirical subspace detector than the STA/LTA. The temporal distribution of the selected events shows that whales are present during the whole survey (Figure 10), with some periods either with more individuals or of higher vocal activity (e.g., 29^{th}–30^{th} January, 2^{nd}–8^{th} February, 9^{th}–11^{th} February, 13^{th}–15^{th} February). Using the high similarity between events, we then automatically picked the newly detected events with the stack. These automatic picks were then manually reviewed resulting in 7156 picks. Out of the 1891 events, 938 events were localized with average horizontal error, vertical error and RMS travel-time residual of $\pm$8.7 km, $\pm$0.9 km and 0.1 s, respectively (Figure 11). Most of the events localized only have a low number of travel-time picks, which lead to larger horizontal uncertainties in comparison with the events detected by the STA/LTA. Focusing on the events localized with uncertainties smaller than $\pm$5 km, these event localizations are similar to those obtained using the events detected with the STA/LTA. The main difference is in the inclusion of more events for days either side of the 29^{th} January. For example, whales are detected on 26^{th} January to the west and in the south half of the network, and on the 2^{nd} February and between the 13^{th} and 15^{th} February mainly in the southwest part of the network. On the 2^{nd} February, an individual or a single group is moving through the network from the southwest to the northeast, ceasing their vocalizations when they reach the center of the network. On the 26^{th} January and between the 13^{th} and 15^{th} February, however, the call localizations are gathered at specific locations.

We then relocalized the events detected by the STA/LTA and the empirical subspace detector using the double-difference method. Most calls were sufficiently linked to other calls to be relocalized due to the high number of instruments deployed and their proximity to the whales. The resulting event relocalizations show that, due to the high linkage between events, more events are retained (i.e., with NonLinLoc only 291 events have uncertainties smaller than ±5 km, Figure 11). In the case of the original events detected by the STA/LTA, 155 events are relocalized with a final average RMS difference time residual of 0.05 s, and preserving ~84% of the differential times in the final relocalizations. Relocalizing all events led to 419 events being relocalized and a final average RMS difference time residual of 0.09 s, and preserving ~45% of the differential times in the final relocalizations. The relocalized events were better clustered both laterally and in depth. Indeed, while some event scatter remains in depth, most events are relocalized at depths shallower than 1 km. On the other hand, some scattered events outside the network couldn't be associated to a cluster and were not kept during the relocalization procedure.

The trajectories of each whale, or groups of whales, during 29th January can be determined (Figure 11). From south to north, estimations of the whale swimming speed for these three main whale tracks are 2.8, 5.0 and 3.1 km/hr (see supplementary material for an animation of whale call localizations during 29th January). In addition, events from 26th January and 2nd February, and at the end of the survey (13th-16th February), are mostly localized in the southwestern part of the network. Those of the 26th January and 2nd February also show a southwest-northeast orientation, which is not the case for those from the 13th-16th February.

IV. DISCUSSION

A. Signal characteristics and whale identification

The main characteristics of the low frequency whale calls we observe during this survey can be summarized as follows:

i) calls have a total duration of 4-5 s with two main parts;

ii) these two main parts have a duration and monochromatic frequency content of ~1-2 s and ~36 Hz and ~2-3 s and ~20 Hz, respectively; and

iii) the calls repeatedly occur over long periods without a precise periodicity.

These characteristics fall within the general range of characteristics for pulsed calls generated by whales (e.g., *Richardson et al., 2013*; *McDonald et al., 2009*). Different baleen whale species inhabit the Eastern Tropical Pacific Ocean including Blue whales, Humpback whales, Bryde's whales, Fin whales, and Minke whales (*Wade & Gerrodette, 1993*; *Palacios et al., 2012*; *Palacios et al., 2023*). Low frequency sounds such as those observed in this study could potentially be associated with some of these baleen whales, such as Blue whales, Humpback whales, Bryde's whales and Fin whales (*Richardson et al., 2013*; *Oleson et al., 2003*).

Similar signals and time-frequency characteristics are reported for Bryde's whales in the Eastern Tropical Pacific Ocean (signals Be1 and Be6 of *Oleson et al., 2003*). Be1 signals show two parts with average frequencies of 21.2 Hz and 36.6 Hz, and an average total duration of 2.7 s. Be6 signals are also very similar to the higher frequency signals observed (e.g., Figures 7 and 9). Other signals attributed to Bryde's whales were reported by *Oleson et al. (2003)*, but they were not observed during our survey. Sightings of Bryde's whales in this region are common even though the abundance is low (*Wade & Gerrodette, 1993*; *Palacios et al., 2012*). Bryde's whales are found all year round within warm and temperate oceans, such as the Eastern Tropical Pacific Ocean, some also migrate within these waters but their actual movements are still largely unknown (*Constantine et al.,* *2018*). We conclude that the most likely origin of the observed signals are Bryde's whales dwelling in this region.

Oleson et al. (2003) suggested that Be1 calls correspond to counter-calling between different whales located relatively close to each other. Our observations with calls alternating between different localizations are consistent with the view that this call is used by the whales to briefly communicate with each other. Moreover, on the 29th January, three whales were simultaneously localized within the network footprint. All the whales show a general trajectory from the southwest to the northeast, with the whale to the far northeast of the network also zigzagging, possibly waiting for the other two individuals. The other two whales finally meet at the eastern edge of the network. The calls could then correspond to the different whales communicating their general location to the other individuals. Even though the calls continue after the two whales met, they are situated outside the network and hence cannot be as precisely localized. Examining the final localizations presented in Figure 11, at least seven Bryde's whales passed through the network at different times, although some whales might have passed through the network more than once. These movements should not be associated with a particular migration, as there is no evidence to support Bryde's whale seasonal migration (*Kato & Perrin, 2009*), but instead a year-round presence is noted in the areas where they have been observed (*Heimlich et al., 2005; McDonald, 2006; Širović et al., 2014*). They might however expand their habitat range seasonally (*Kerosky et al., 2012; Ferreira et al., 2021*).

The higher frequency Be6 signal is generally of lower amplitude and is hence recorded only by nearby OBSs, which suggests that it only propagates over shorter distances. This seems to support the suggestion of *Oleson et al. (2003)*, that these signals were produced by closely spaced animals while heading in a specific direction. The examples shown in Figures 7 and 9 correspond to calls produced on the 14th February (red dots in Figure 11), and their different amplitudes observed at nearby instruments seems to indicate they were generated by more than one animal. On this day, 111 low-frequency calls were localized, mostly in a cluster centered around the position of OBS NG-24 (Figure 1). Their spatial distribution as a compact cluster might, however, be a consequence of the limited number of OBSs remaining on the seabed at this time (five OBSs: 4, 7, 14, 17 and 24 – Figure 1).

B. Methodological aspects

Whale calls are generally detected in the time-frequency domain owing to their stable, recognizable time-frequency features (e.g., *Mellinger & Clark, 2000*; *Munger et al., 2005*; *Baumgartner & Mussoline, 2011*). Such detectors can use pre-defined time-frequency templates to target particular signals or scan spectrogram portions for any high-magnitude features. Matched filtering techniques do not take into account potential variations due to changes in time-frequency features (i.e., over time and/or across a population), background noise, or site-specific noise levels for example. General time-frequency and time-domain detectors (e.g., the STA/LTA) are more flexible at the expense of their sensitivity, and require additional steps to select and classify the signals (*Baumgartner & Mussoline, 2011*). For the STA/LTA, high amplitude noise, even outside the frequency band of interest can mask the signals to be detected. On the other hand, subspace detectors take into account some signal variability embedded within the original signal dataset and translate it to the vector basis used to perform the detection (*Harris, 2006*). The selectivity of this vector basis allows the detection of signals with lower signal-to-noise ratio compared to other general time-domain detectors. Different factors determine the final performance of this technique such as using a representative set of signals to build the vector basis, using an appropriate number of singular vectors, and adequately setting the detection threshold. Further studies would be needed to compare the performance of time-domain subspace detectors with those of frequency-domain template matching detectors.

Even though we used the STA/LTA approach on OBS geophone data, we managed to detect high-amplitude whale calls. However, using a larger number of OBS hydrophones and the VA hydrophones as well as the empirical subspace detector, we obtained roughly 10 times more events. This shows the benefit of both using hydrophones and subspace detection techniques to study whale vocalizations. The observation of whale calls during the whole recording period shows that they are continuously present at one position or another (Figure 10). The number of detections obtained using the STA/LTA and the empirical subspace detector also strongly depends on other factors such as the presence of seismic shots and/or intense noise episodes in the data (e.g., on the 2nd February), and the number of stations available at different times. Most of the OBSs and the VA are deployed until the 2nd February whereas, after that date and until the end of the survey, only five OBSs and the VA remain deployed in the network. Nevertheless, some calls were detected during the whole survey.

Despite the high number of OBSs at the beginning of the survey, the average horizontal uncertainty for the calls detected using the STA/LTA and the empirical subspace detector remain relatively high (i.e., at 2.1 and 8.7 km, respectively). This likely mainly arises from the challenges of the travel-time picking discussed earlier. This could also indicate discrepancies between the observed travel-times and the theoretical arrival times of the first P-wave calculated using the eikonal equation (*Lomax et al., 2009*). In the case of strong bathymetry variations, such as those encountered around mid-ocean ridges, ray paths between whales and instruments on the seafloor might not be direct but involve reflections from the seabed or within the water column (*Dréo et al., 2019*). This can be particularly important for longer propagation paths. Call localizations in depth are well-constrained for calls within the instrument network until the partial instrument recovery on the 1st February, 2015. However, calls localized deeper than 0.5-1 km are systematically associated with larger vertical uncertainties (e.g., 0.5-1 km) and generally a lower number of time picks as well. For calls occurring after the 2nd February, their uncertainty increases due to the lower number of instruments remaining deployed and their linear deployment configuration. This can be counterbalanced for some calls using the double-difference method when event clustering is high and, hence, due to the high connectivity between nearby events. Ultimately, although localization error remains, our approach has resulted in a general improvement in ability to reconstruct the general trend of the whale movement trajectories, estimate of their number, and interpret of their behavior.

V. CONCLUSION

In this study we analyze and compare continuous data acquired by 25 OBSs and a VA of 12 hydrophones deployed around the CRR, Eastern Tropical Pacific Ocean, in January and February 2015. The noise levels observed for the hydrophones closer to the seafloor are on average 10 dB higher than for those situated higher up in the water column. Calls and seismic events are generally localized using instruments either close to the sea surface or at the seafloor. The VA provides a larger aperture in depth that could, in theory, improve the localization accuracy in this dimension. In this study, however, depth uncertainties remained high (e.g., ~ $\pm$0.8 km) even for calls including travel-time picks from the VA data.

We observe two different signal types produced by whales during this deployment. The first is present during the whole deployment with different amplitudes and recurrences. It displays two parts with consistent frequency content; the first is a 1-2 s long signal of high amplitude and frequency ~36 Hz, and the second is a 2-3 s long signal of generally lower amplitude and frequency ~20 Hz. The second type of signal is a 0.5-1.0 s long signal of low amplitude and higher frequency content ranging between 80 and 160 Hz. Both types of signals are most likely made by Bryde's whales, a whale species thought to inhabit and is occasionally sighted in this region. The first signal type seems to correspond to whales counter-calling between each other to provide their approximate location, and eventually meeting up to form a group. The second could not be associated with specific conditions or type of behavior.

Using highly similar whale calls previously detected using the STA/LTA approach, we employed the network empirical subspace detector and obtained approximately 10 times more events (i.e., 188 vs 1891, respectively). These events were then absolutely localized and finally relocalized using the double-difference technique. The combination of the subspace detector with the double-difference technique results in an increase in events localized and a better delineation of the whale trajectory. This is particularly effective for highly similar events observed by our dense instrument network as that leads to highly linked events. These precise relocalizations show that at least seven (group of) whales passed through the network at different times, most of them from the southwest to the northeast (i.e., from an area closer to the Galapagos Islands towards the southern shores of Panama). At the end of the survey period, one or more whales stayed within the area for up to a few days. This could, however, be a localization artifact due to the limited number of instruments remaining deployed at the end of the survey and their generally, north-south linear orientation. Regardless, this study illustrates the value of applying advanced detection and localization methods in the passive monitoring of baleen whales, particularly their ways of communicating and ecology, which is crucial to their identification, conservation and the mitigation of the potential impacts of human activities.

SUPPLEMENTARY MATERIAL

See supplementary material at [URL] for an animation of the final whale call localizations obtained on the 29th January, 2015, between 2pm and 10pm.

ACKNOWLEDGMENTS

We acknowledge funding from the Natural Environmental Research Council (NERC) via grant NE/1027010/1 and support from the DYLCAN project of the Universidad de Los Andes (J. B. T.). We would like to thank all those involved in the planning and acquisition of data during the OSCAR research cruises JC113, JC114 and SO238, including the officers, engineers and crew of the RRS James Cook and the FS Sonne, the scientific party, and all seagoing technicians and engineers. The NERC Ocean-Bottom Instrumentation Facility (*Minshull et al., 2005*) also provided technical support at sea. We thank two anonymous reviewers for their valuable comments. CAV thanks MINCIENCIAS for funding through grant project 80740-182-2021, and the Universidad Nacional de Colombia through projects Hermes 51307 and 57879. The Generic Mapping Tool (GMT) was used for the first figure of this article.

AUTHOR DECLARATIONS

Conflict of Interest

The authors declare no conflict of interest.

DATA AVAILABILITY

Data from cruises JC113, JC114 and SO238 are archived at the NERC's British Oceanographic Data Centre and are available from the following links:

JC113 – www.bodc.ac.uk/resources/inventories/cruise_inventory/report/15035/,

JC114 – www.bodc.ac.uk/resources/inventories/cruise_inventory/report/15036/, and

SO238 – www.bodc.ac.uk/resources/inventories/cruise_inventory/report/15045/.

REFERENCES

Banyte, D., Morales Maqueda, M.A., Smeed, D.A., Hobbs, R., Megann, A., and Recalde, S. (**2018a**). "Geothermal heating in the Panama Basin: 1. Hydrography of the basin", J. Geophys. Res. Oceans **123**(10), 7382-7392.

Banyte, D., Morales Maqueda, M.A., Smeed, D.A., Megann, A., Hobbs, R., and Recalde, S. (**2018b**). "Geothermal heating in the Panama Basin. Part II: Abyssal water mass transformation", J. Geophys. Res. Oceans **123**(10), 7393-7406.

Barrett, S.A., and Beroza, G.C. (**2014**). "An empirical approach to subspace detection", Seismol Res. Lett. **85**(3), 594-600.

Baumgartner, M. F., and Mussoline, S. E. (**2011**). "A generalized baleen whale call detection and classification system", The Journal of the Acoustical Society of America **129**(5), 2889-2902.

Brodie, D. C., & Dunn, R. A. (**2015**). "Low frequency baleen whale calls detected on ocean-bottom seismometers in the Lau basin, southwest Pacific Ocean", The Journal of the Acoustical Society of America **137**(1), 53-62.

Constantine, R., Iwata, T., Nieukirk, S.L., and Penry, G.S. (**2018**). "Future directions in research on Bryde's whales", Frontiers in Marine Science **5**, 333.

De La Hoz, C., Tary, J. B., and Lomax, A. (**2021**). "Empirical subspace detection applied to triggered seismicity by the July 25, 2011, M_w 5.0 earthquake in the Sea of Marmara, Turkey", Computers & Geosciences **152**, 104738.

Dréo, R., Bouffaut, L., Leroy, E., Barruol, G., and Samaran, F. (**2019**). "Baleen whale distribution and seasonal occurrence revealed by an ocean bottom seismometer network in the Western Indian Ocean", Deep Sea Research Part II: Topical Studies in Oceanography **161**, 132-144.

Dunn, R. A., and Hernandez, O. (**2009**). “Tracking blue whales in the eastern tropical Pacific with an ocean-bottom seismometer and hydrophone array”, The Journal of the Acoustical Society of America **126**(3), 1084-1094.

Ferreira, R., Dinis, A., Badenas, A., Sambolino, A., Marrero-Pérez, J., Crespo, A., and Alves, F. (**2021**). “Bryde's whales in the North-East Atlantic: New insights on site fidelity and connectivity between oceanic archipelagos”, Aquatic Conservation: Marine and Freshwater Ecosystems **31**(10), 2938-2950.

Frankel, A.S. (**2009**). Sound production. In “Encyclopedia of marine mammals” (Academic Press, Cambridge), pp. 1056-1071.

Funnell, M.J., Robinson, A.H., Hobbs, R.W. and Peirce, C. (**2021**). “Evolution and properties of young oceanic crust: constraints from Poisson’s ratio”, Geophysical Journal International **225**(3), 1874-1896.

Harris, D. (**2006**). Subspace Detectors: Theory, Lawrence Livermore Natl. Lab. Rep. UCRL- TR-222758. Lawrence Livermore National Laboratory, Livermore, California.

Heimlich, S. L., Mellinger, D. K., Nieukirk, S. L., and Fox, C. G. (**2005**). “Types, distribution, and seasonal occurrence of sounds attributed to Bryde’s whales (Balaenoptera edeni) recorded in the eastern tropical Pacific, 1999–2001”, The Journal of the Acoustical Society of America **118**(3), 1830-1837.

Gregory, E.P.M. (**2018**). The seismic characterisation of layer 2 in oceanic crust around ODP borehole 504B (PhD thesis). University of Durham, UK.

Hatch, L.T., Clark, C.W., Van Parijs, S.M., Frankel, A.S., and Ponirakis, D.W. (**2012**). “Quantifying loss of acoustic communication space for right whales in and around a US National Marine Sanctuary”, Conservation Biology **26**(6), 983-994.

Hobbs, R., and Peirce, C. (**2015**). RRS James Cook JC114 Cruise Report. Online Report. https://www.bodc.ac.uk/resources/inventories/cruise_inventory/reports/jc114.pdf.

Kato, H., and Perrin, W. F. (**2009**). "Bryde's whales: Balaenoptera edeni/brydei", in Encyclopedia of marine mammals (pp. 158-163). Academic Press.

Kavanagh, A. S., Owen, K., Williamson, M. J., Blomberg, S. P., Noad, M. J., Goldizen, A. W., ... and Dunlop, R. A. (**2017**). "Evidence for the functions of surface-active behaviors in humpback whales (Megaptera novaeangliae)", Marine Mammal Science **33**(1), 313-334.

Kerosky, S. M., Širović, A., Roche, L. K., Baumann-Pickering, S., Wiggins, S. M., and Hildebrand, J. A. (**2012**). "Bryde's whale seasonal range expansion and increasing presence in the Southern California Bight from 2000 to 2010", Deep Sea Research Part I: Oceanographic Research Papers **65**, 125-132.

Lomax, A., Zollo, A., Capuano, P., and Virieux, J. (**2001**). "Precise, absolute earthquake location under Somma-Vesuvius volcano using a new three-dimensional velocity model", Geophys. J. Int. **146**(2), 313–331.

Lomax, A., Michelini, A., and Curtis, A. (**2009**). Earthquake Location, Direct, Global-Search Methods, in Encyclopedia of Complexity and System Science, vol. 5. Springer, New York, pp. 2449-2473.

Lowell, R.P., Zhang, L., Maqueda, M.A.M., Banyte, D., Tong, V.C.H., et al. (**2020**). "Magma-hydrothermal interactions at the Costa Rica Rift from data collected in 1994 and 2015", Earth Planet. Sci. Lett. **531**, 115991.

Matias, L., and Harris, D. (**2015**). "A single-station method for the detection, classification and location of fin whale calls using ocean-bottom seismic stations", The Journal of the Acoustical Society of America **138**(1), 504-520.

Mellinger, D. K., and Clark, C. W. (**2000**). "Recognizing transient low-frequency whale sounds by spectrogram correlation", The Journal of the Acoustical Society of America **107**(6), 3518-3529.

McDonald, M. A., Hildebrand, J. A., and Webb, S. C. (**1995**). "Blue and fin whales observed on a seafloor array in the Northeast Pacific", The Journal of the Acoustical Society of America **98**(2), 712-721.

McDonald, M.A., Hildebrand, J.A., and Mesnick, S. (**2009**). "Worldwide decline in tonal frequencies of blue whale songs", Endangered species research **9**(1), 13-21.

McDonald, M.A., Mesnick, S.L., and Hildebrand, J.A. (**2006**). "Biogeographic characterization of blue whale song worldwide: using song to identify populations", Journal of cetacean research and management **8**(1), 55-65.

Minshull, T.A., Sinha, M.C., and Peirce, C. (**2005**). "Multi-disciplinary, sub-seabed geophysical imaging", Sea Technol. **46**, 27-31.

Munger, L. M., Mellinger, D. K., Wiggins, S. M., Moore, S. E., and Hildebrand, J. A. (**2005**). "Performance of spectrogram cross-correlation in detecting right whale calls in long-term recordings from the Bering Sea", Canadian Acoustics **33**(2), 25-34.

Oleson, E.M., Barlow, J., Gordon, J., Rankin, S., and Hildebrand, J.A. (**2003**). "Low frequency calls of Bryde's whales", Marine Mammal Science **19**(2), 407-412.

Palacios, D.M., Herrera, J.C., Gerrodette, T., Garcia, C., Soler, G.A., Avila, I.C., Bessudo, S., Hernandez, E., Trujillo, F., Forez-Gonzalez, L., and Kerr, I. (**2012**). "Cetacean distribution and relative abundance in Colombia's Pacific EEZ from survey cruises and platforms of opportunity", J. Cetacean Res. Manage. **12**(1), 45-60.

Palacios, D., Felix, F., Montecinos, Y., Najera, E., Kelez, S., Samaniego, J., Velásquez, P., Zapata, L., Lancaster, M., Friedlaender, A.S., Castro, C.A., Quintana, E., Bermúdez-Rivas, C., Cazas, JJ., Villamil Echeverri, C., Rojas Bracho, L., Sepúlveda, M., Medrano-Gonzales, L., Santillan, L., Aguilar Arakaki, R., Pineda, L., Reisinger, R., and Johnson, C.M. (**2023**). Blue Corridor of the Eastern Pacific: Opportunities and Actions for the protection of Migratory Whales. A Technical Report. World Wide Fund for Nature (WWF).

Peirce, C., Tedd, J. C., and Hobbs, R. W. (**2023**). "Structure and dynamics of the Ecuador Fracture Zone, Panama Basin", Geophys. J. Int. **235**(2), 1519-1540.

Richardson, W. J., Greene Jr, C. R., Malme, C. I., and Thomson, D. H. (**2013**). *Marine mammals and noise* (Academic press, Cambridge).

Robinson, A.H., Zhang, L., Hobbs, R.W., Peirce, C., and Tong, V.C.H. (**2020**). "Magmatic and tectonic segmentation of the intermediate-spreading Costa Rica Rift – a fine balance between magma supply rate, faulting, and hydrothermal circulation", Geophys. J. Int. **222**, 132-152.

Širović, A., Bassett, H. R., Johnson, S. C., Wiggins, S. M., and Hildebrand, J. A. (**2014**). "Bryde's whale calls recorded in the Gulf of Mexico", Marine Mammal Science **30**(1), 399-409.

Širović, A., Hildebrand, J.A., Wiggins, S.M., McDonald, M.A., Moore, S.E., and Thiele, D. (**2004**). "Seasonality of blue and fin whale calls and the influence of sea ice in the Western Antarctic Peninsula", Deep Sea Research Part II: Topical Studies in Oceanography **51**(17-19), 2327-2344.

Socheleau, F.-X., Leroy, E., Carvallo Pecci, A., Samaran, F., Bonnel, J., and Royer, J.-Y. (**2015**). "Automated detection of Antarctic blue whale calls", J. Acoust. Soc. Am. **138**(5), 3105-3117.

Song, F., Warpinski, N.R., Toksöz, M.N., and Kuleli, H.S. (**2014**). "Full-waveform based microseismic event detection and signal enhancement: an application of the subspace approach", Geophys. Prospect. **62**(6), 1406-1431.

Tary, J.B., Herrera, R.H., Han, J., and van der Baan, M. (**2014**). "Spectral estimation—What is new? What is next?", Reviews of Geophysics **52**(4), 723-749.

Tary, J. B., Hobbs, R. W., Peirce, C., Lesmes, C. L., and Funnell, M. J. (**2021**). "Local rift and intraplate seismicity reveal shallow crustal fluid-related activity and sub-crustal faulting", Earth and Planetary Science Letters **562**, 116857.

Tenorio-Hallé, L., Thode, A. M., Sarkar, J., Verlinden, C., Tippmann, J., Hodgkiss, W. S., and Kuperman, W. A. (**2017**). "A double-difference method for high-resolution acoustic tracking using a deep-water vertical array", The Journal of the Acoustical Society of America **142**(6), 3474-3485.

Vargas, C.A., Pulido, J.E., and Hobbs, R.W. (**2018**). "Thermal structure of the Panama Basin by analysis of seismic attenuation", Tectonophysics **730**, 81–99.

Wade, P.R., and Gerrodette, T. (**1993**)." Estimates of cetacean abundance and distribution in the eastern tropical Pacific", Report of the International Whaling Commission **43**, 477-493.

Waldhauser, F., and Ellsworth, W.L. (**2000**). "A double-difference earthquake location algorithm: Method and application to the northern Hayward fault, California", Bulletin of the seismological society of America **90**(6), 1353-1368.

Wilcock, W. S. (**2012**). "Tracking fin whales in the northeast Pacific Ocean with a seafloor seismic network", The Journal of the Acoustical Society of America, **132**(4), 2408-2419.

Wilcock, W. S., and Hilmo, R. S. (**2021**). "A method for tracking blue whales (Balaenoptera musculus) with a widely spaced network of ocean bottom seismometers", Plos one **16**(12), e0260273.

Wilson, D.J., Robinson, A.H., Hobbs, R.W., Peirce, C., and Funnell, M.J. (**2019**). "Does intermediate spreading-rate oceanic crust result from episodic transition between magmatic and magmadominated, faulting-enhanced spreading?–the Costa Rica Rift example", Geophys. J. Int. **218**, 1617-1641.